Science Advances
AAAS

Supplementary Materials for

Anti-phagocytosis-blocking repolarization-resistant membrane-fusogenic liposome (ARMFUL) for adoptive cell immunotherapy

Chunxiong Zheng *et al.*

Corresponding author: Fangfang Cao, cffdc@nus.edu.sg; Yu Tao, taoy28@mail.sysu.edu.cn; Xiaoyuan Chen, chen.shawn@nus.edu.sg; Mingqiang Li, limq567@mail.sysu.edu.cn

Sci. Adv. **9**, eadh2413 (2023)
DOI: 10.1126/sciadv.adh2413

The PDF file includes:

Other Supplementary Material for this manuscript includes the following:

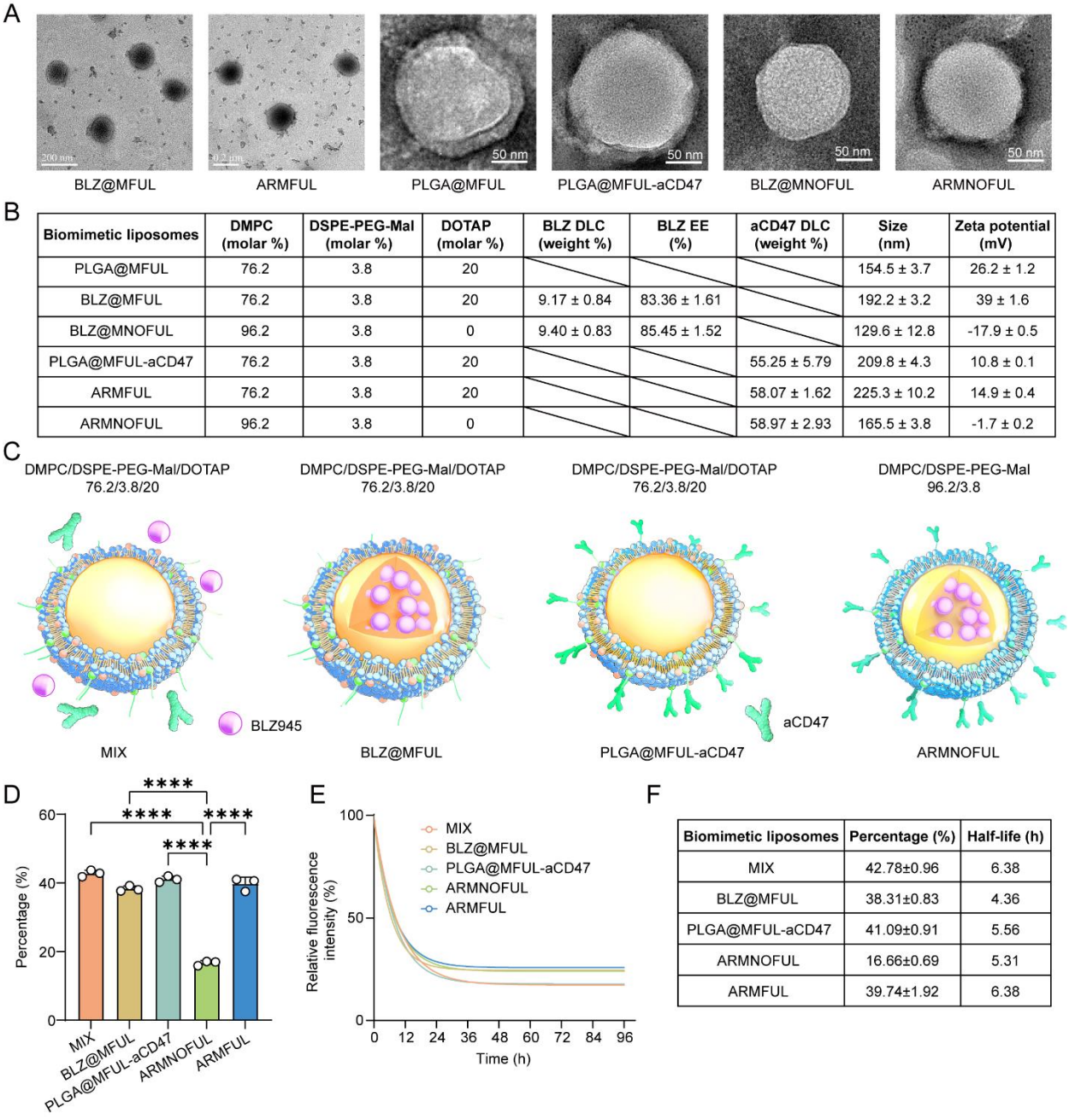

Biomimetic liposomes	DMPC (molar %)	DSPE-PEG-Mal (molar %)	DOTAP (molar %)	BLZ DLC (weight %)	BLZ EE (%)	aCD47 DLC (weight %)	Size (nm)	Zeta potential (mV)
PLGA@MFUL	76.2	3.8	20				154.5 ± 3.7	26.2 ± 1.2
BLZ@MFUL	76.2	3.8	20	9.17 ± 0.84	83.36 ± 1.61		192.2 ± 3.2	39 ± 1.6
BLZ@MNOFUL	96.2	3.8	0	9.40 ± 0.83	85.45 ± 1.52		129.6 ± 12.8	-17.9 ± 0.5
PLGA@MFUL-aCD47	76.2	3.8	20			55.25 ± 5.79	209.8 ± 4.3	10.8 ± 0.1
ARMFUL	76.2	3.8	20			58.07 ± 1.62	225.3 ± 10.2	14.9 ± 0.4
ARMNOFUL	96.2	3.8	0			58.97 ± 2.93	165.5 ± 3.8	-1.7 ± 0.2

Biomimetic liposomes	Percentage (%)	Half-life (h)
MIX	42.78±0.96	6.38
BLZ@MFUL	38.31±0.83	4.36
PLGA@MFUL-aCD47	41.09±0.91	5.56
ARMNOFUL	16.66±0.69	5.31
ARMFUL	39.74±1.92	6.38

Fig. S1. Characterization of ARMFUL and the contrastive nanoparticles.

(**A**), TEM images of the BLZ@MFUL, ARMFUL, PLGA@MFUL, PLGA@MFUL-aCD47, BLZ@MNOFUL, and ARMNOFUL. (**B**), Physicochemical characterizations of six different biomimetic liposomes. DLC, drug loading capacity. EE, encapsulation efficiency. (**C**), Schematic representation of other interventions including MIX, PLGA@MFUL-aCD47, BLZ@MFUL, and ARMNOFUL. (**D**), The percentage of liposomes that successfully get into the macrophages. (**E**), The half-life curves of liposomes. (**F**), The summarization of the percentage and half-life of liposomes. Data are presented as means ± SD, n = 6 (**B**) or 3 (**D**, **F**) biologically independent samples. Statistical significance is calculated by t-test: * $p < 0.05$, ** $p < 0.01$, *** $p < 0.001$ and **** $p < 0.0005$.

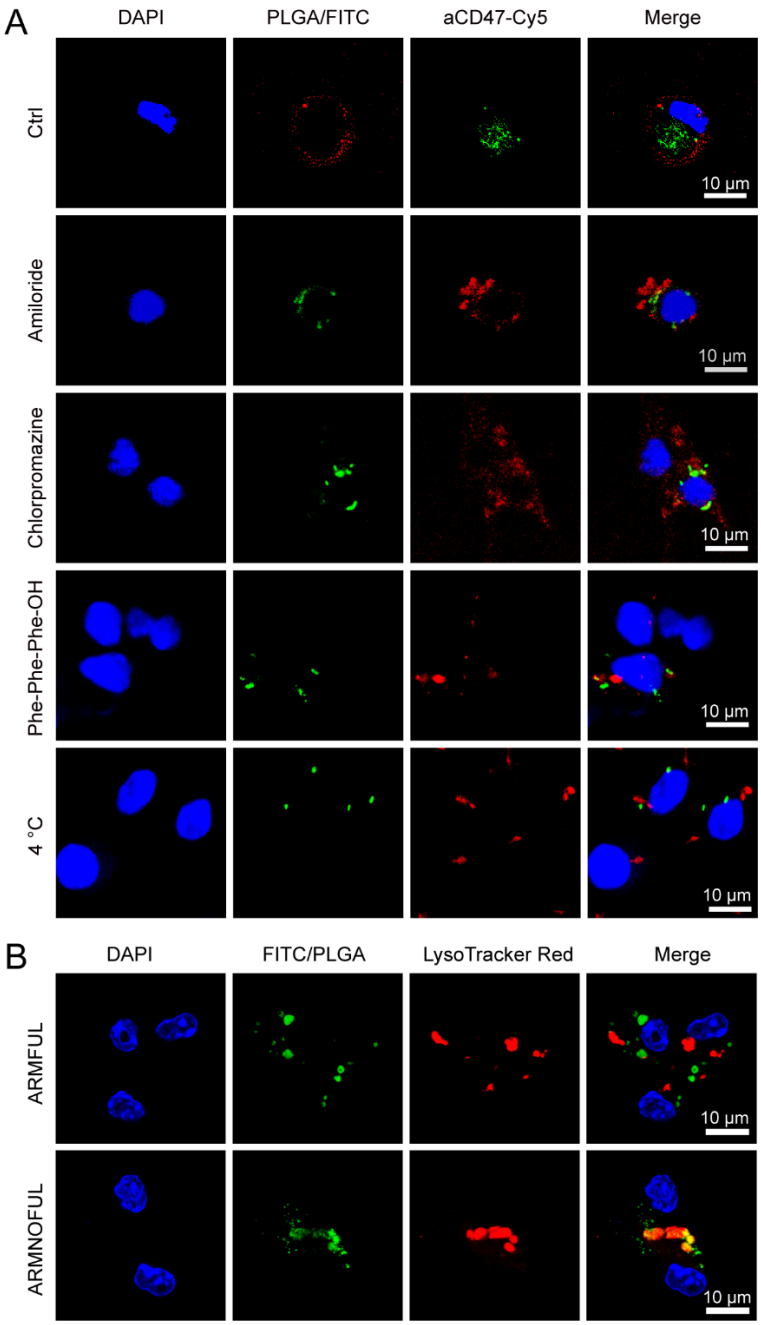

Fig. S2. Confocal laser scanning microscopy (CLSM) images of bone marrow-derived macrophages (BMDMs) after incubation with ARMFUL.

(**A**), CLSM images of BMDMs after treatment with cell-uptake inhibitors. Blue fluorescence: nuclei stained with DAPI; green fluorescence: FITC-labeled PLGA-based polymeric core; and red fluorescence: Cy5-labeled aCD47. (**B**), CLSM images of BMDMs after incubation with FITC@ARMFUL and FITC@ARMNOFUL. Blue fluorescence: nuclei stained with DAPI; green fluorescence: FITC/PLGA core; and red fluorescence: LysoTracker Red DND-99.

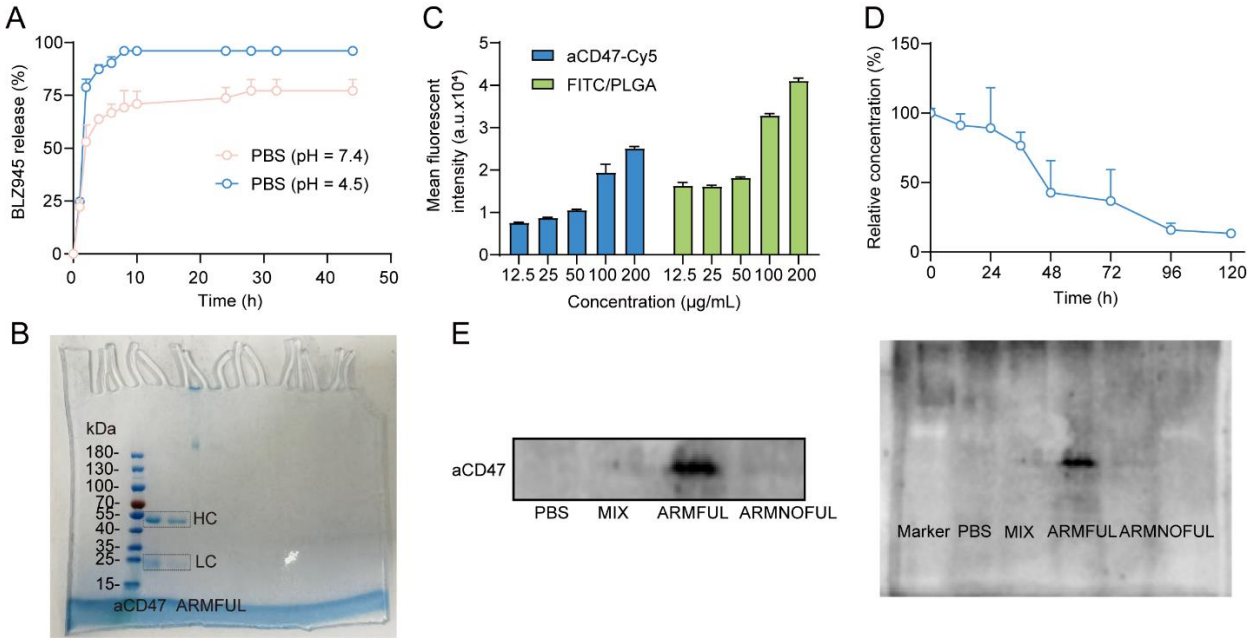

Fig. S3. Release profile, gel electrophoresis analysis and cell uptake of ARMFUL.

(**A**), Accumulative release of BLZ945 from PLGA cores in the PBS (pH 7.4 or 4.5). (**B**), Gel electrophoresis showing the heavy chain (HC) and light chain (LC) released from free aCD47 and ARMFUL. The gel was stained with Coomassie Brilliant Blue. The molecular weights of HC and LC are approximately 50 kDa and 25 kDa, respectively. (**C**), Mean fluorescent intensity of BMDMs after incubation with FITC@ARMFUL-Cy5. 1×10^6 BMDMs were treated with different concentrations of biomimetic liposomes. (**D**), The relative content of BLZ945 in the macrophages after ARMFUL engineering. BLZ945 concentration in the cells was detected by high-performance liquid chromatography (HPLC). (**E**), Western blot analysis of aCD47 on the cell membrane after treatment with PBS, MIX, ARMFUL, and ARMNOFUL. Data represent mean ± SD, n = 3 biologically independent samples.

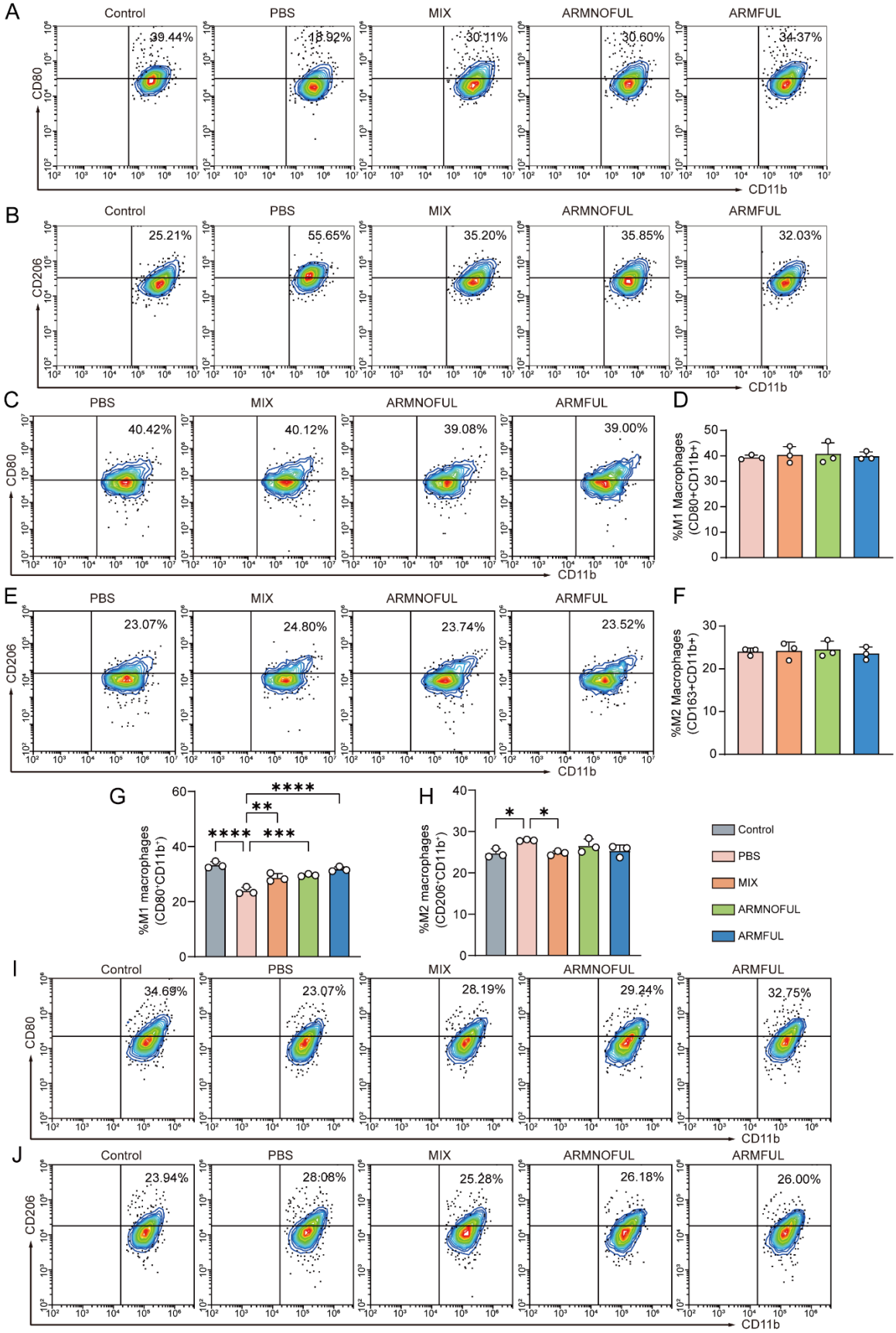
A
Control
PBS
MIX
ARMNOFUL
ARMFUL
39.44%
13.92%
30.11%
30.60%
34.37%
CD80
CD11b
B
25.21%
55.65%
35.20%
35.85%
32.03%
CD206
C
40.42%
40.12%
39.08%
39.00%
D
%M1 Macrophages (CD80+CD11b+)
E
23.07%
24.80%
23.74%
23.52%
F
%M2 Macrophages (CD163+CD11b+)
G
%M1 macrophages (CD80+CD11b+)
H
%M2 macrophages (CD206+CD11b+)
Control
PBS
MIX
ARMNOFUL
ARMFUL
I
34.69%
23.07%
28.19%
29.24%
32.75%
J
23.94%
28.08%
25.28%
26.18%
26.00%

Fig. S4. Fluorescence-activated cell sorting (FACS) analysis of M1/M2-related biomarkers on macrophages after treatment with the medium containing IL-4.

(**A**, **B**), Engineered BMDMs were stimulated with IL-4 for 24 h. The graphs of M1 ($CD80^+CD11b^+$) (**A**) and M2 ($CD206^+CD11b^+$) macrophages (**B**) were analyzed by flow cytometry. (**C**, **D**, **E**, **F**), The level of M1 ($CD80^+CD11b^+$) (**C**, **D**) and M2 ($CD206^+CD11b^+$) (**E**, **F**) markers before treatment with IL-4. The cells were gated from $F4/80^+CD11b^+$ populations in the FACS profile. (**G**, **H, I, J**), The percent of M1 ($CD80^+CD11b^+$) (**G**, **I**) and M2 ($CD206^+CD11b^+$) (**H**, **I**) populations in engineered macrophages after treatment with B16F10 tumor cell conditioned medium, respectively. The cells were gated from $F4/80^+CD11b^+$ populations in the FACS profile. Data represent mean ± SD, n = 3 biologically independent samples. Statistical significance was calculated by one-way ANOVA with Dunnett's multiple comparison tests: * $p < 0.05$, ** $p < 0.01$, *** $p < 0.001$ and **** $p < 0.0005$.

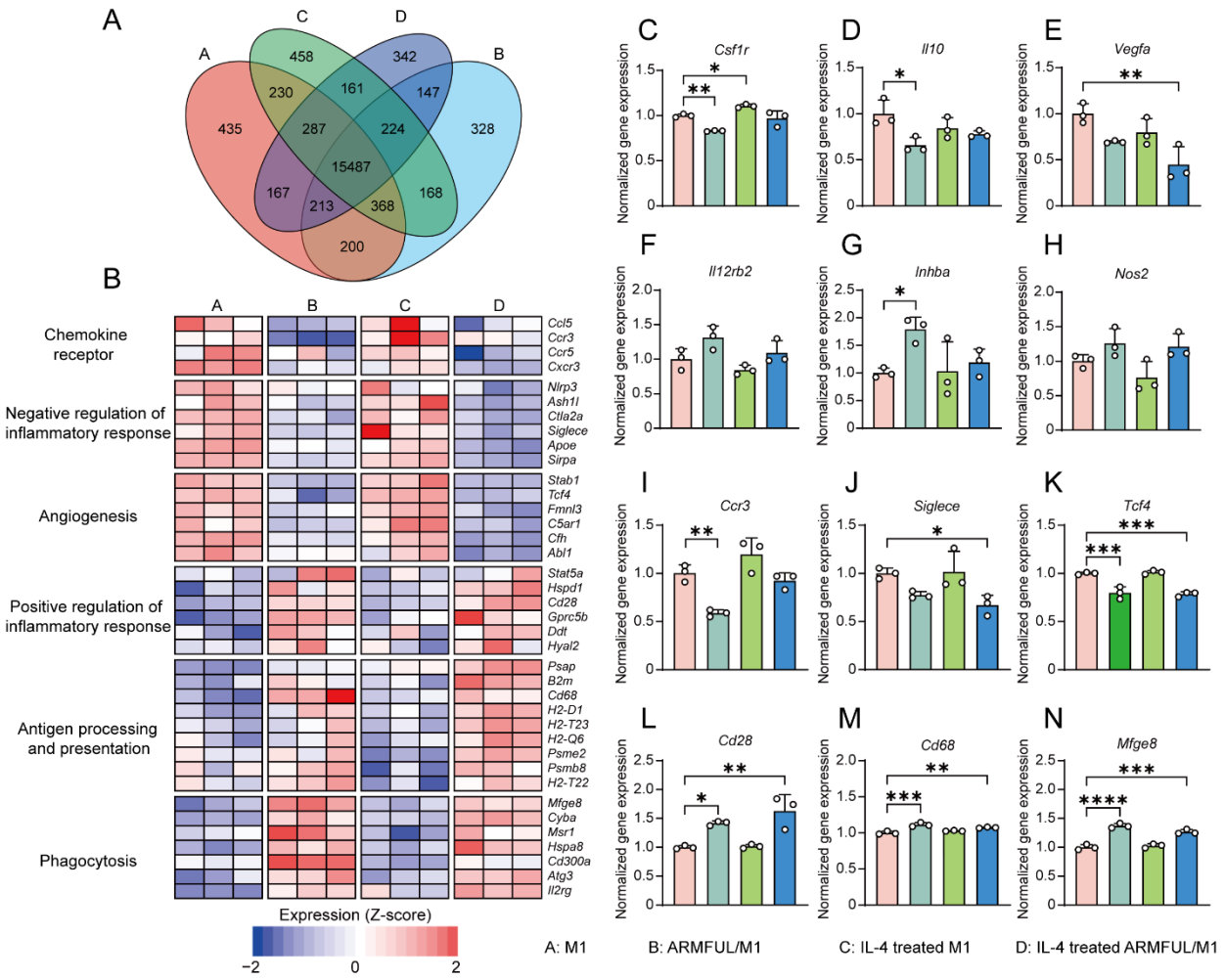

Fig. S5. RNA sequencing analysis of native M1 macrophages and ARMFUL/M1 with/without IL-4 treatment.

(**A**), Venn diagram of the whole expressed genes. (**B**), Expression of selected genes related to chemokine receptor, negative regulation of inflammatory response, angiogenesis, positive regulation of inflammatory response, antigen processing and presentation, and phagocytosis in M1 macrophages and engineered M1 macrophages with/without IL-4 treatment (n = 3/group). (**C-N**), Normalized gene expression of representative genes based on counts. Data represent mean ± SD (**C-N**). Statistical significance by one-way ANOVA with Dunnett's multiple comparison tests: * $p < 0.05$, ** $p < 0.01$, *** $p < 0.001$ and **** $p < 0.0005$.

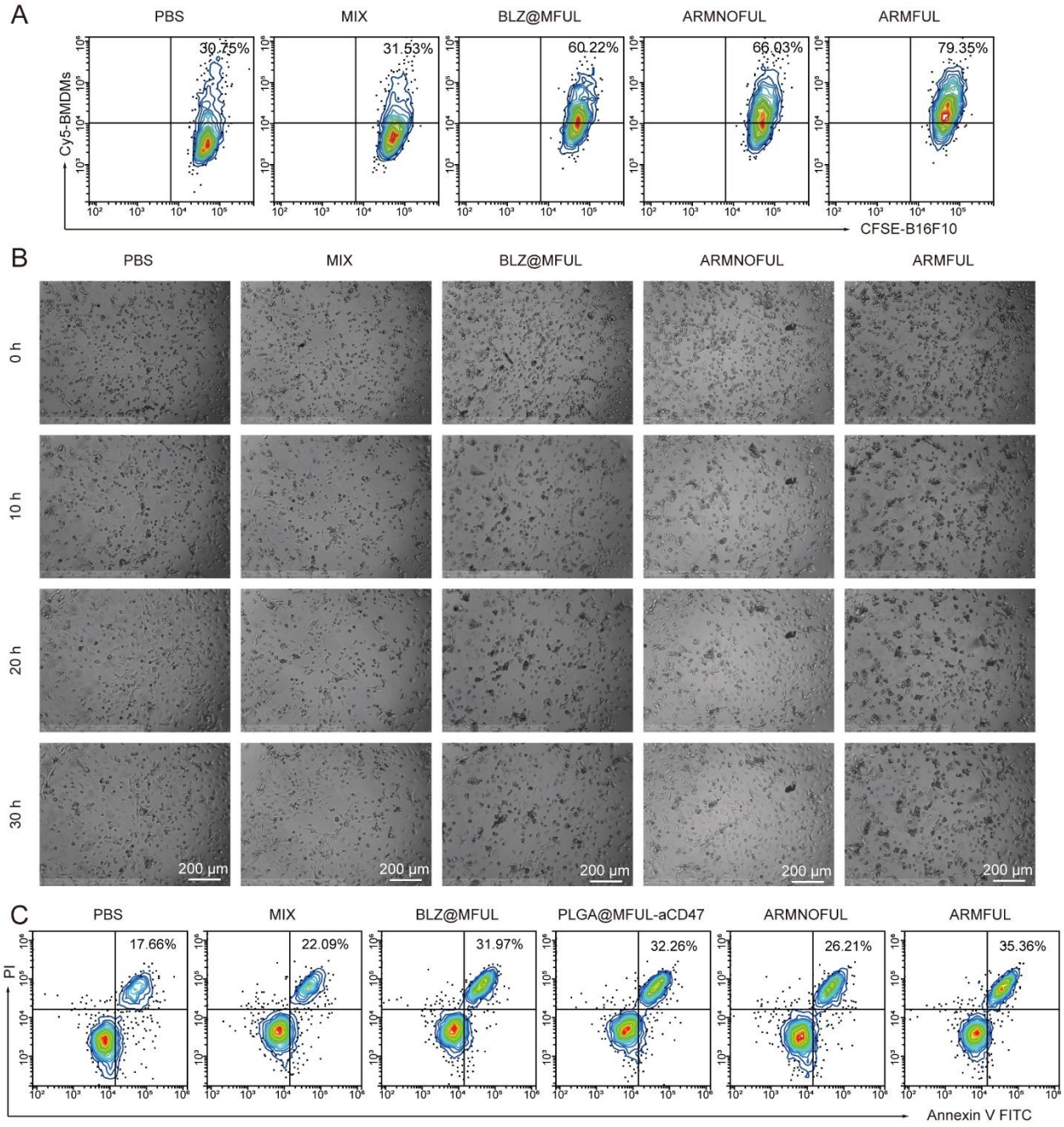

Fig. S6. The enhanced phagocytosis ability of ARMFUL/M1.

(**A**), The percentage of macrophages phagocytosing B16F10 cancer cells. Macrophages were labeled with DSPE-PEG-Cy5, while B16F10 cancer cells were labeled with CFSE. The cells were gated from $CFSE^{+}$ populations in the FACS profile. (**B**), Representative images of macrophages phagocytosing B16F10 cancer cells at 0, 10, 20, and 30 h. The views were recorded through a live cell dynamic imaging and analysis system every 10 minutes for 36 h. (**C**), The apoptosis percentage of B16F10 cells after coculturing with engineered BMDMs. The cells were treated with Annexin V-FITC/PI Apoptosis Detection Kit, then analyzed for Annexin V and PI staining on a flow cytometer and calculated apoptosis.

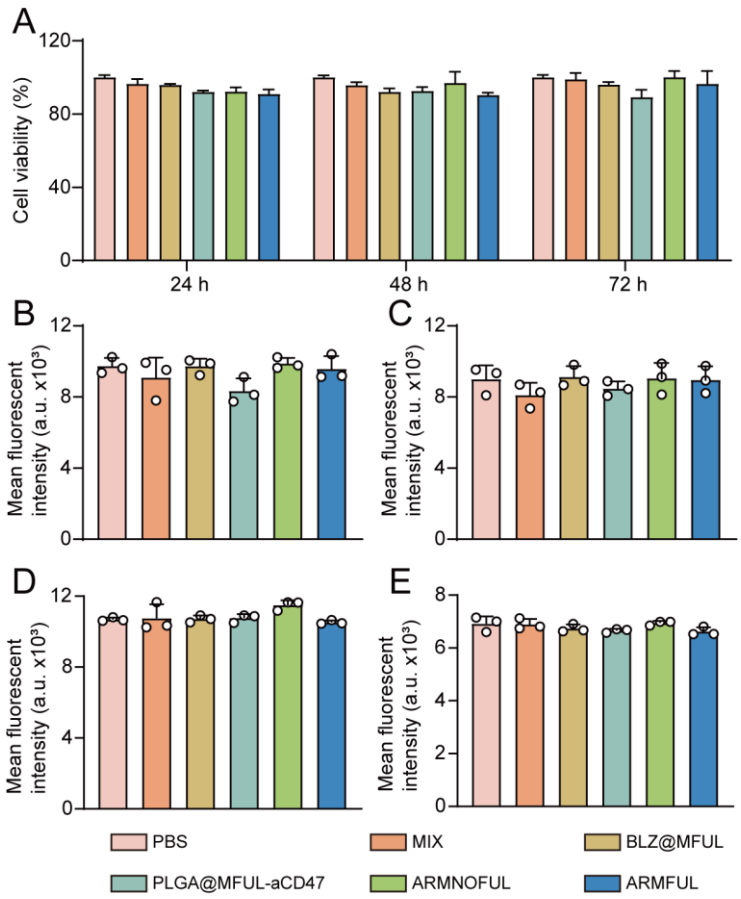

Fig. S7. Cell viability of BMDMs after ARMFUL engineering and its potential effect on macrophage functions.

(**A**), Cell viability of engineered BMDMs at 24, 48, and 72 h after treatment with ARMFUL, determined by CCK-8 assays. There was no significance between groups within 72 h, indicating the good biocompatibility of ARMFULs. (**B**, **C**), The expression of iNOS (**B**) and HIF-1α (**C**) on macrophages engineered with different liposomes. (**D**, **E**), The expression of TLR2 (**D**) and TLR4 (**E**) in M1 macrophages after engineering with different liposomes. Data represent mean ± SD, n = 3 biologically independent samples.

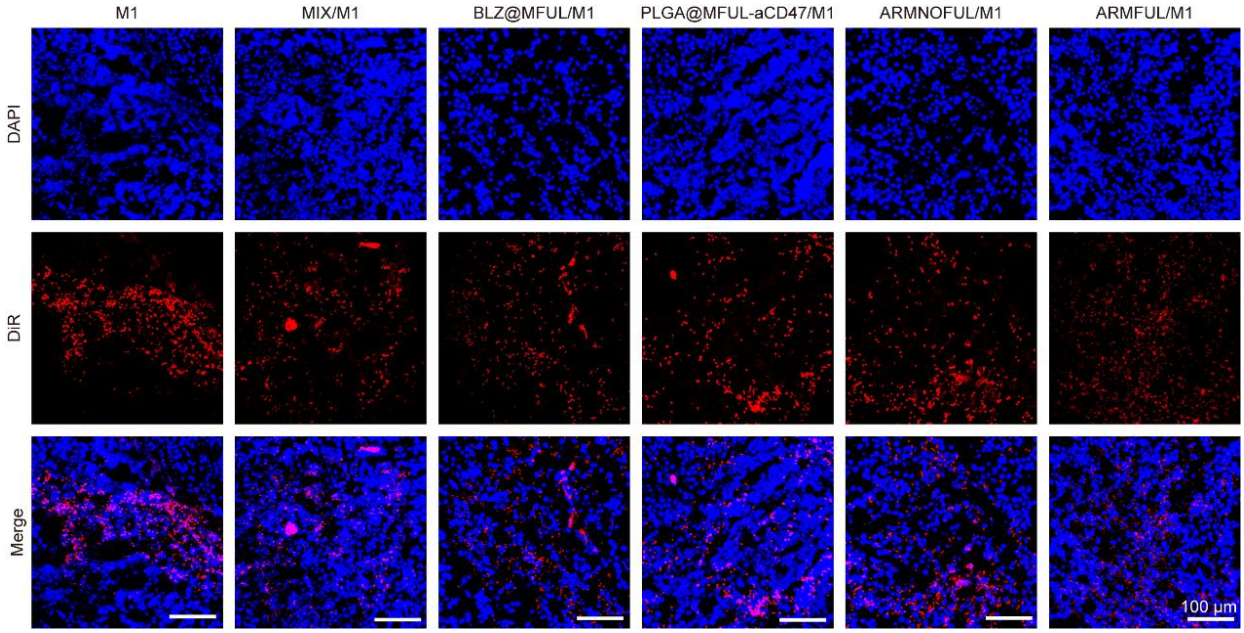

Fig. S8. CLSM images of tumor tissues from mice treated with DiR-labelled ARMFUL/M1.

The CLSM images of tumor tissue slices showed that engineered macrophages could infiltrate into tumors effectively. Blue fluorescence: nuclei stained with DAPI; Red fluorescence: macrophages stained with DiR.

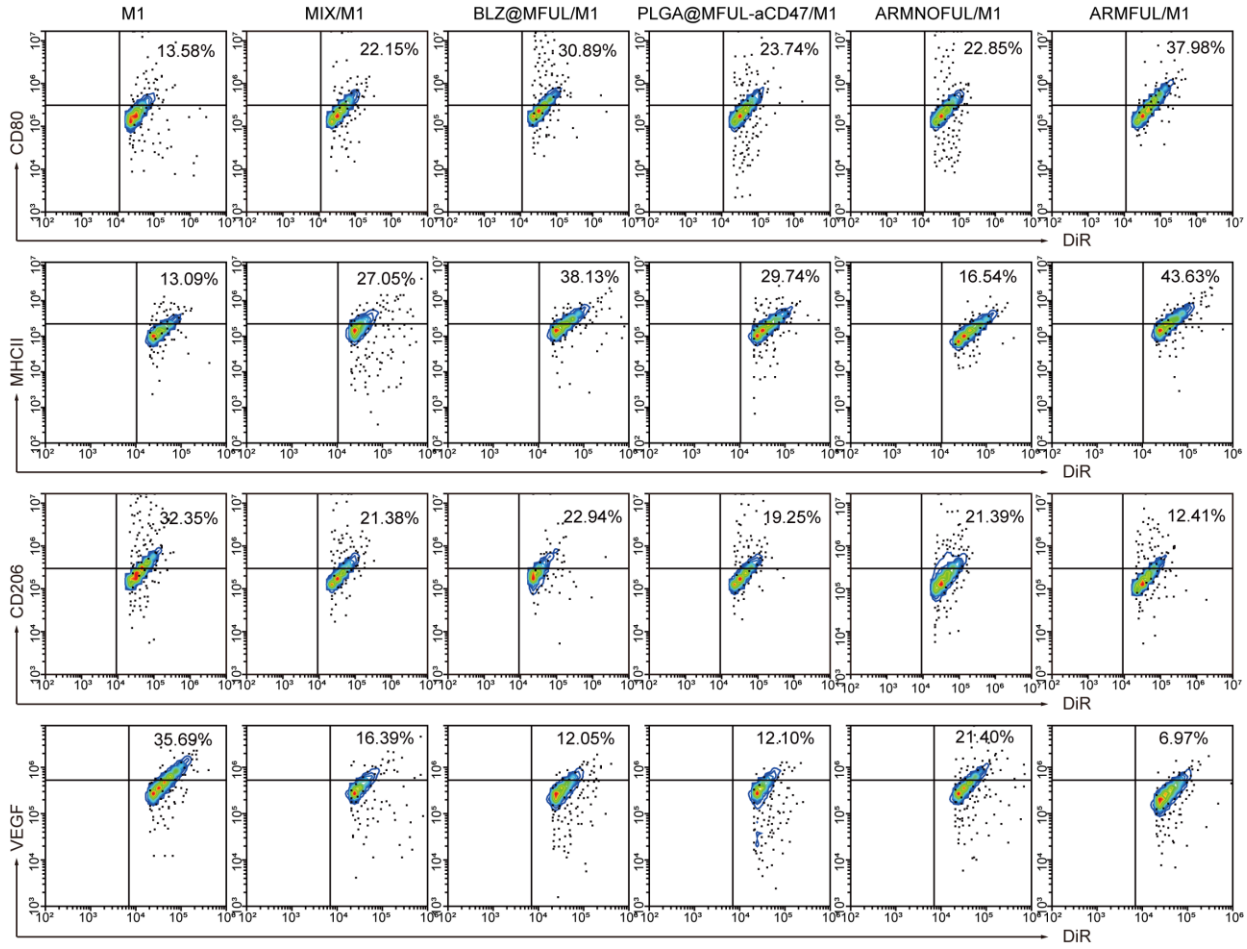

Fig. S9. The percentage of CD80$^+$, MHCII$^+$, CD206$^+$, and VEGF$^+$ populations in adoptively transferred macrophages in tumors.

The cells were gated from F4/80$^+$DiR$^+$ populations in the FACS profile.

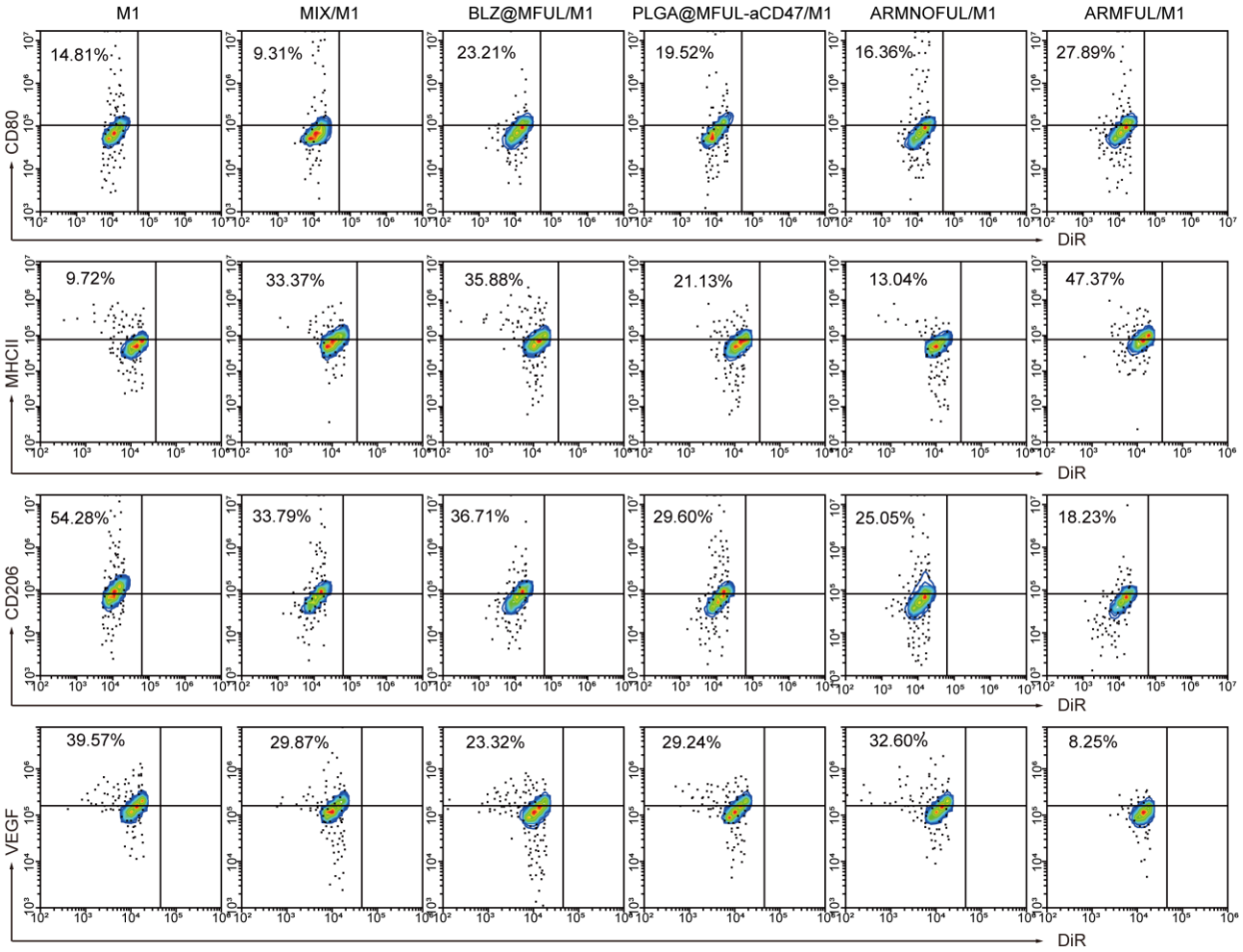

Fig. S10. The percentage of CD80$^+$, MHCII$^+$, CD206$^+$, and VEGF$^+$ cells in tumor-associated macrophages in tumors.

The cells were gated from F4/80$^+$DiR$^-$ populations in the FACS profile.

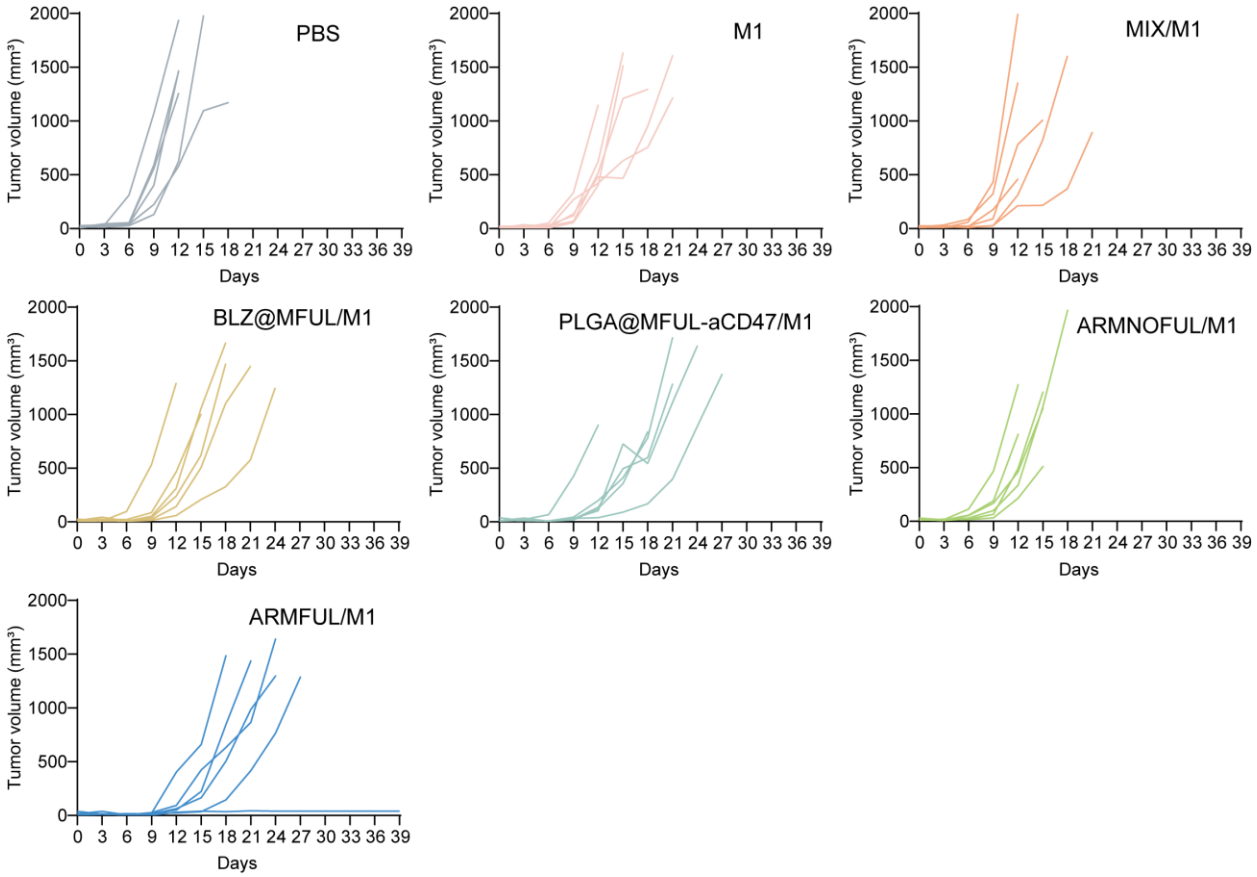

Fig. S11. Growth curves of tumors in individual mice burdened with B16F10-Luc cells after intravenous injection of PBS, M1 macrophages, and engineered M1 macrophages.

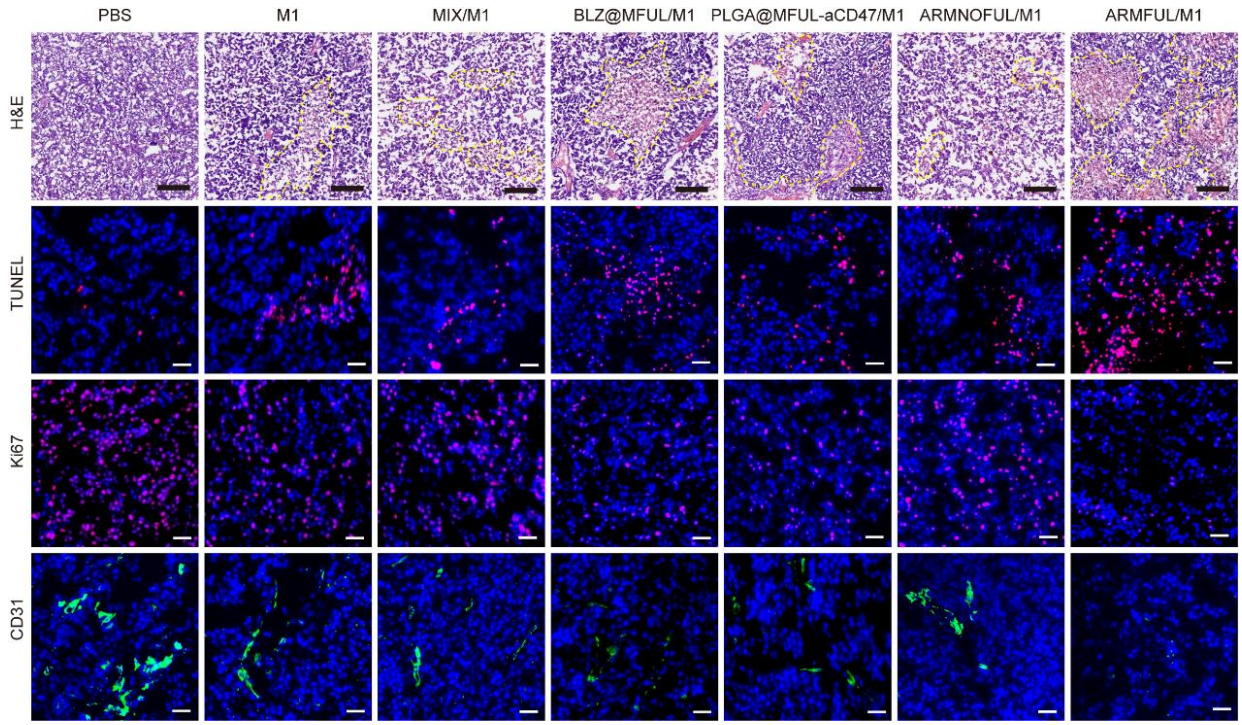

Fig. S12. Immunohistochemical and immunofluorescence analysis of tumor tissues.

Representative H&E staining images and immunofluorescence staining images for TUNEL (red), Ki67 (red), and CD31 (green) of tumor slices from mice burdened with B16F10-Luc cells after intravenous injection of PBS, M1 macrophages, and engineered M1 macrophages. The scale bar is 200 μm.

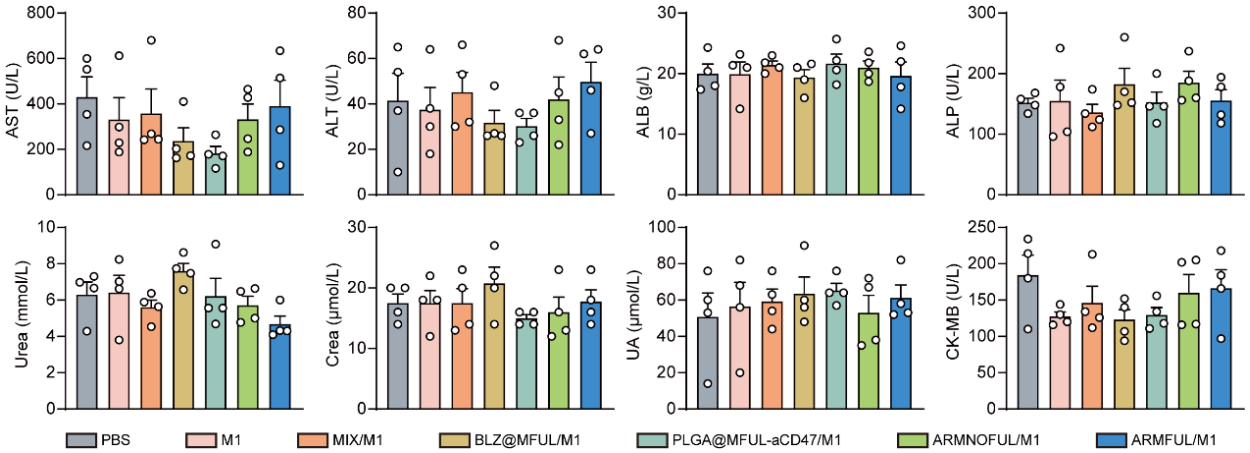

Fig. S13. Serum biochemical analysis of mice treated with ARMFUL/M1.

Serum biochemical parameters of mice burdened with B16F10-Luc cells after treatment, including aspartate transaminase (AST), alanine transaminase (ALT), albumin (ALB), alkaline phosphatase (ALP), urea nitrogen (Urea), creatinine (Crea), uric acid (UA), and creatine kinase-MB (CK-MB), n = 4 biologically independent mice.

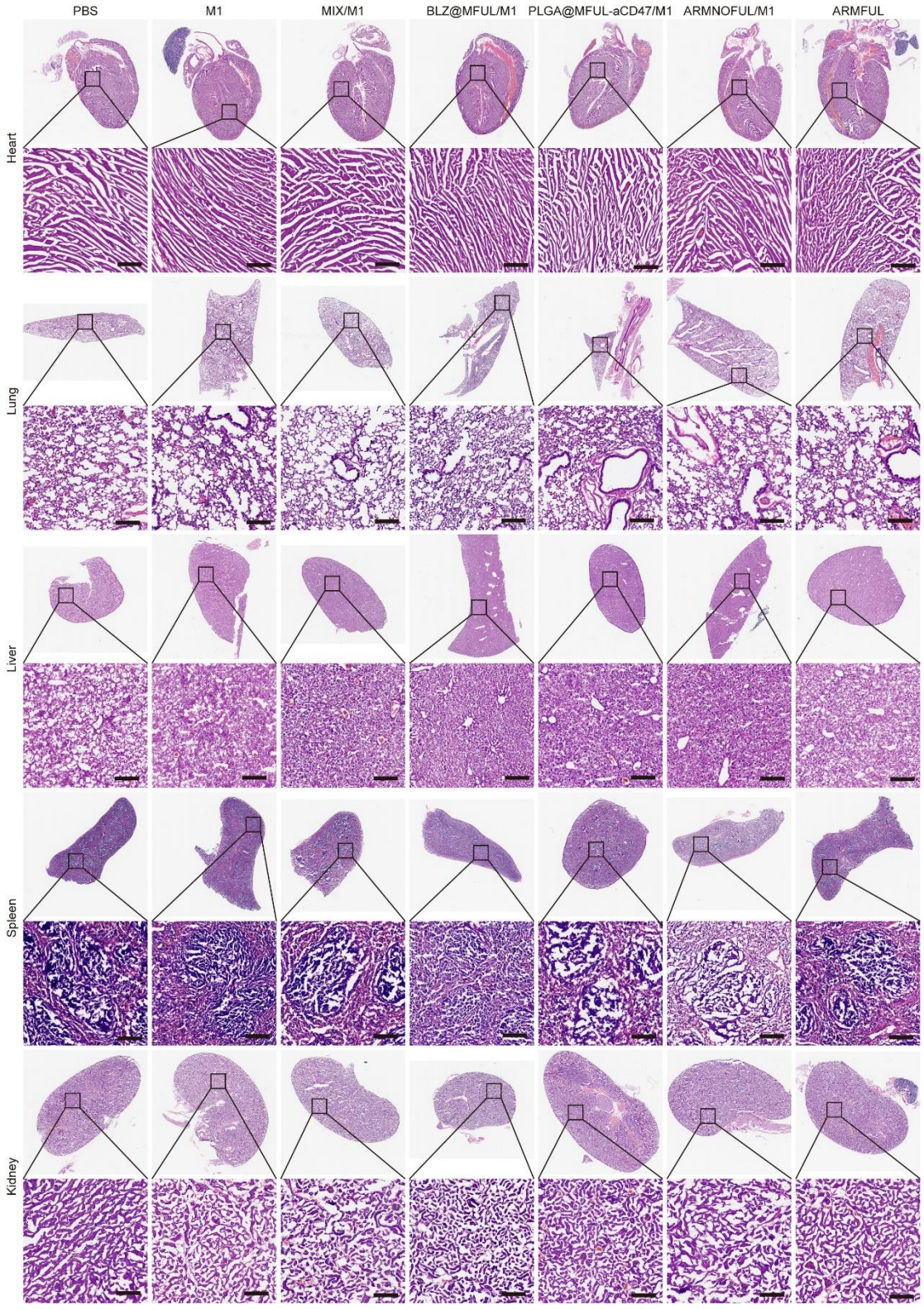

Fig. S14. Immunohistochemical analysis for tissue damage.

H&E staining images of major organ slices from mice burdened with B16F10-Luc cells after treatment. The scare bar is 200 μm.

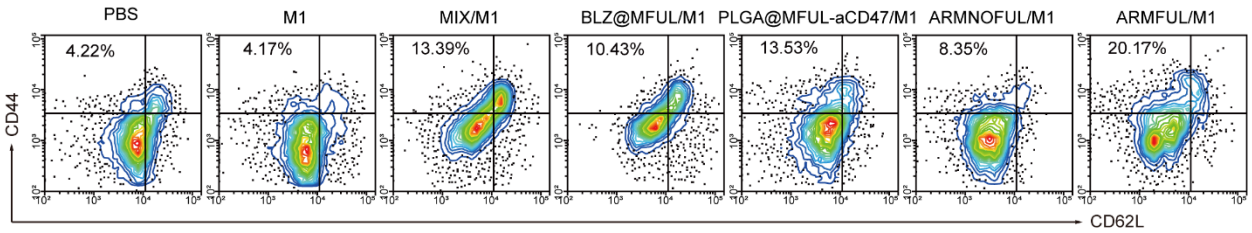

Fig. S15. The percentage of effector memory T cells in the spleen.

The $CD62^{-}CD44^{+}$ T cells were gated from $CD45^{+}CD4^{+}$ populations in the FACS profile.

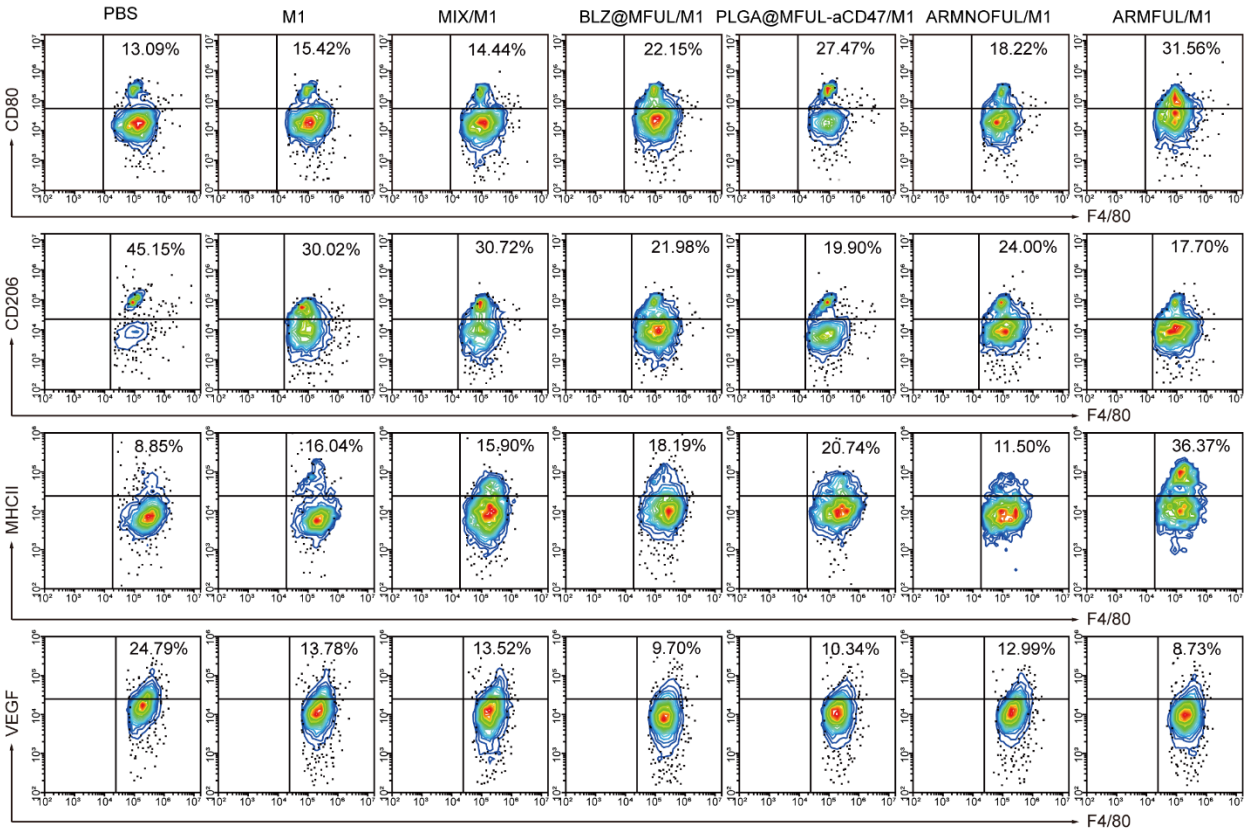

Fig. S16. The percentage of CD80$^+$, MHCII$^+$, CD206$^+$, and VEGF$^+$ macrophages in tumors. The cells were gated from CD45$^+$F4/80$^+$CD11b$^+$ populations in the FACS profile.

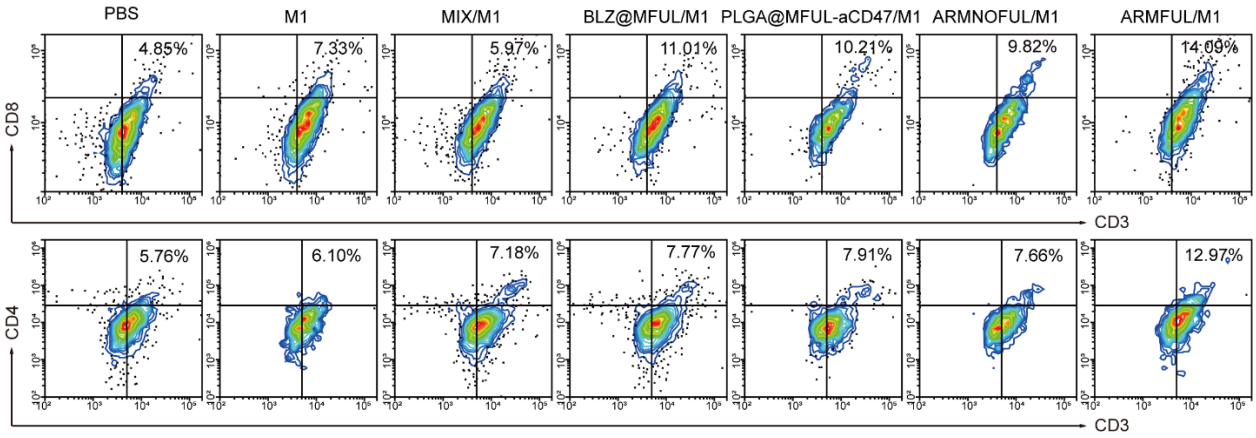

Fig. S17. The percentage of $CD8^+$ and $CD4^+$ T cells in tumors.

The cells were gated from $CD45^+$ populations in the FACS profile.

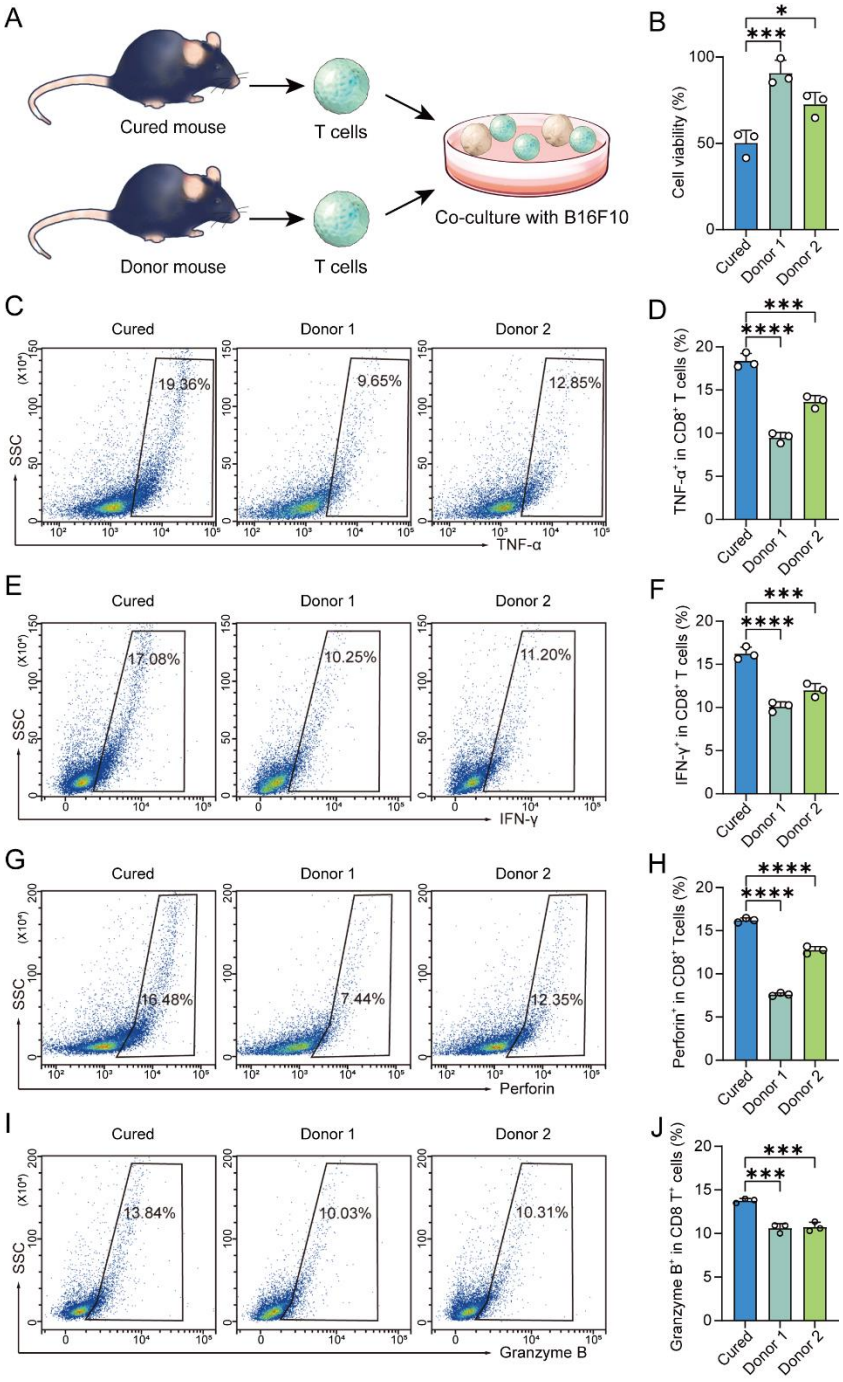

Fig. S18. Systemic immunological memory after BMFL-engineered M1 macrophage treatment.

(**A**), Schematic representation of the systemic immunological memory assay. T cells were isolated from the spleen of the cured or same-age donor mice, then co-cultured with B16F10-Luc cells. (**B**), Cell viability of B16F10-Luc cells after incubation with T cells. (**C**-**J**), The percentage of TNFα^{+}, IFNγ^{+}, perforin^{+}, and granzyme B^{+} T cell after co-culturing with B16F10-Luc cells. Data represent mean ± SD (**D**, **F**, **H**, **J**). Statistical significance was calculated by one-way ANOVA with Dunnett's multiple comparison tests: * $p < 0.05$, ** $p < 0.01$, *** $p < 0.001$, and **** $p < 0.0005$.

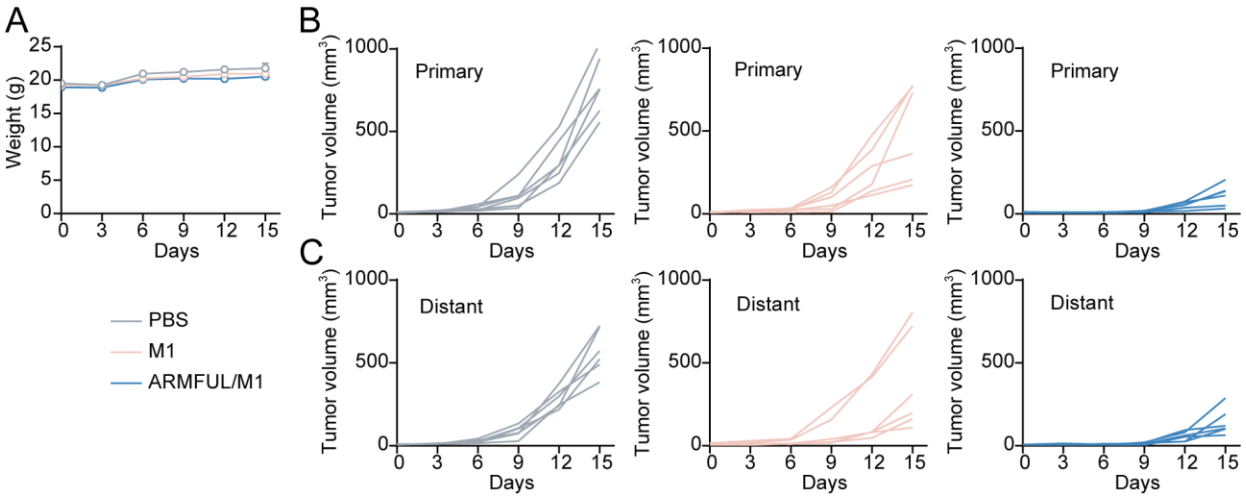

Fig. S19. Weight change and individual tumor growth curve of mice.

(A), Weight change of mice burdened with B16F10 cells after treatment (n = 6/group). (**B)**, Growth curves of tumors in individual mice burdened with B16F10 cells after intratumor injection of PBS, M1 macrophages, and engineered M1 macrophages (n = 6/group).

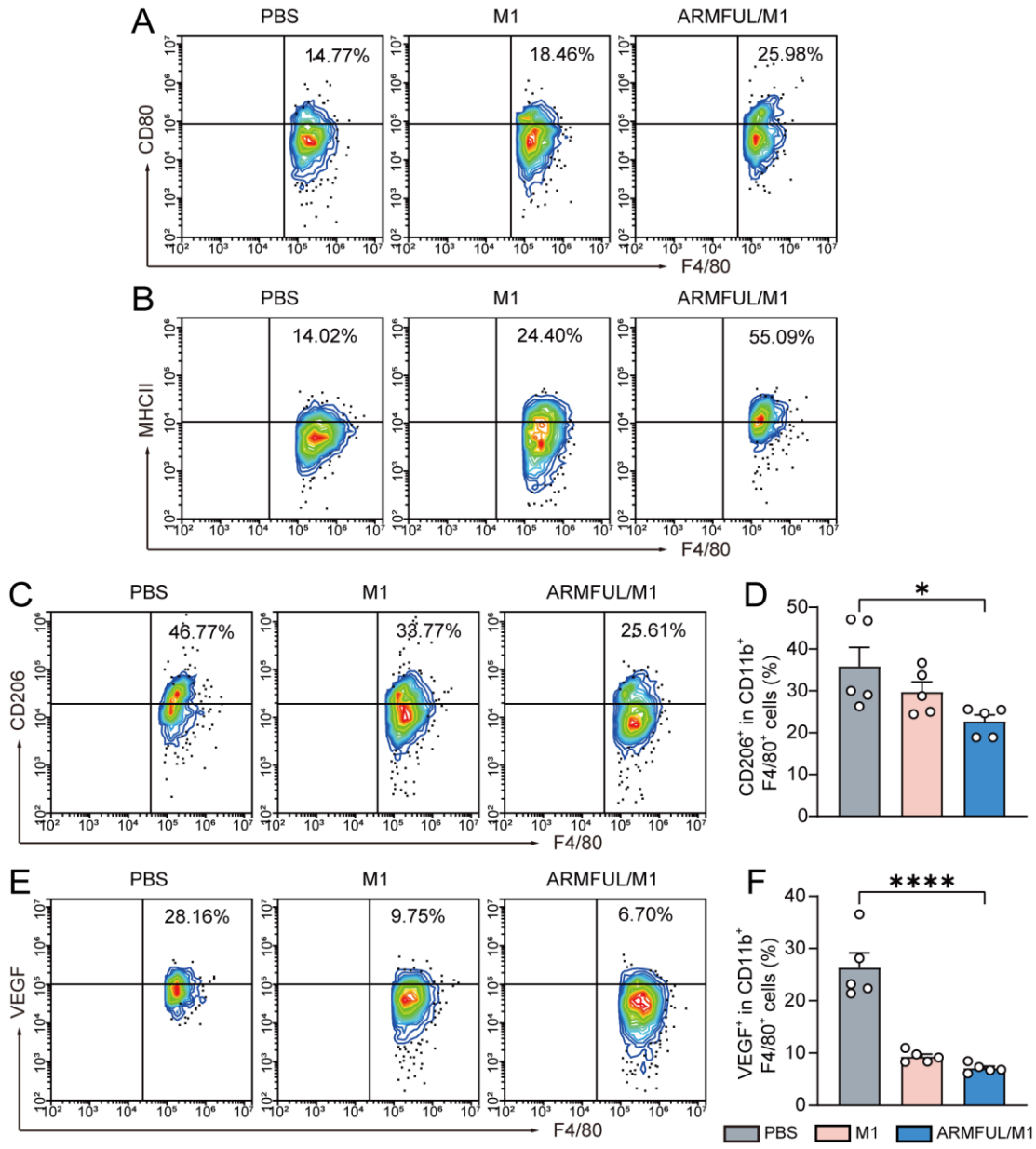

Fig. S20. FACS analysis of macrophage phenotypes in primary tumors.

(**A**, **B**), The percentage of $CD80^+$, $MHCII^+$ macrophages in primary tumors. (**C**, **D**), The percentage of $CD206^+$ macrophages in primary tumors. (**E**, **F**), The percentage of $VEGF^+$ macrophages in primary tumors. The cells were gated from $CD45^+F4/80^+CD11b^+$ populations in the FACS profile. Data represent mean ± SD (**D**, **F**), n = 5 biologically independent mice. Statistical significance by one-way ANOVA with Dunnett's multiple comparison tests: * $p < 0.05$, ** $p < 0.01$, *** $p < 0.001$ and **** $p < 0.0005$.

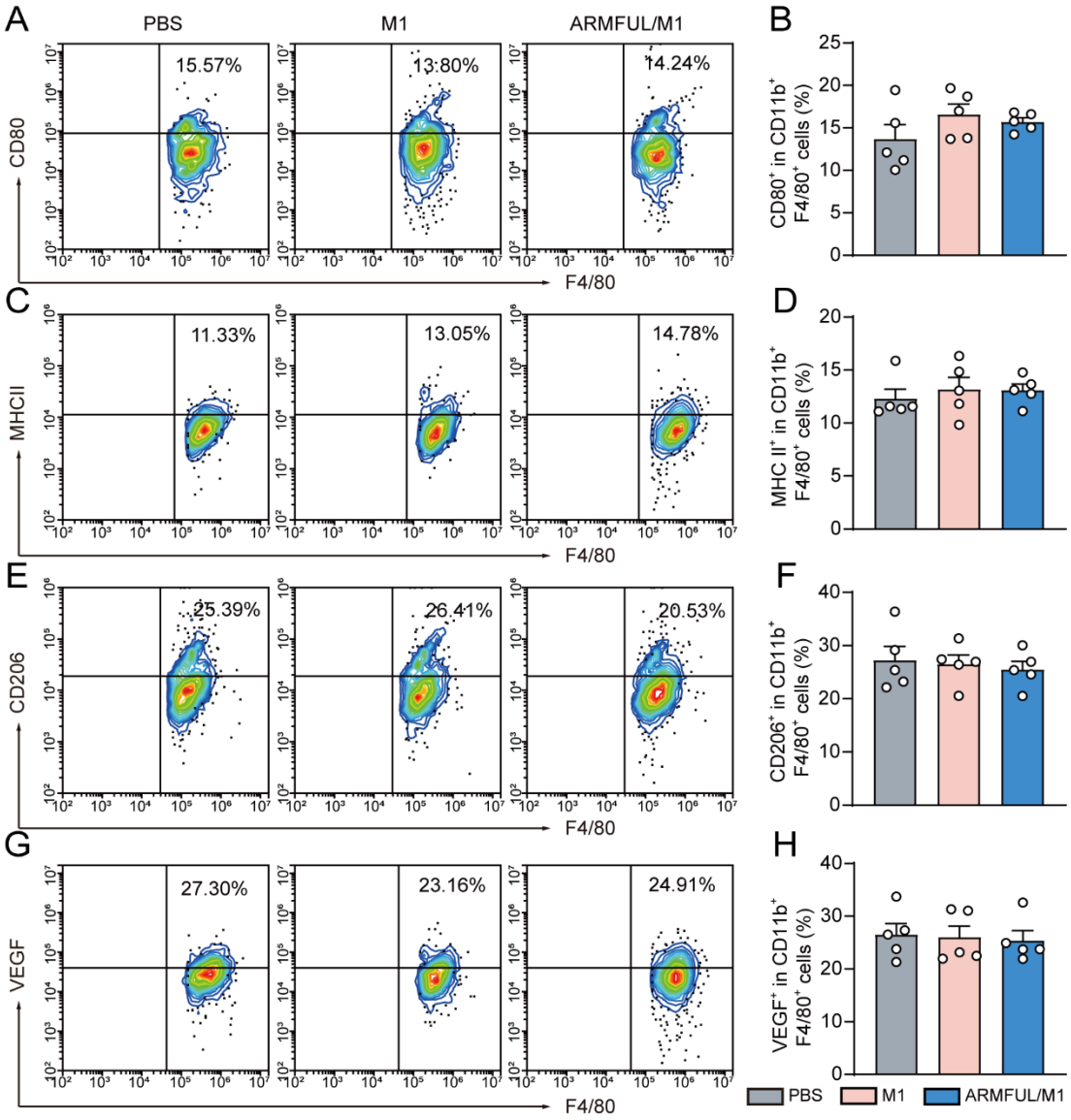

Fig. S21. FACS analysis of macrophage phenotypes in distant tumors.

(**A**-**H**), The percentage of $CD80^+$, $MHCII^+$, $CD206^+$, and $VEGF^+$ macrophages in distant tumors. The cells were gated from $CD45^+F4/80^+CD11b^+$ populations in the FACS profile. Data represent mean ± SD (**B**, **D**, **F**, **H**), n = 5 biologically independent mice.

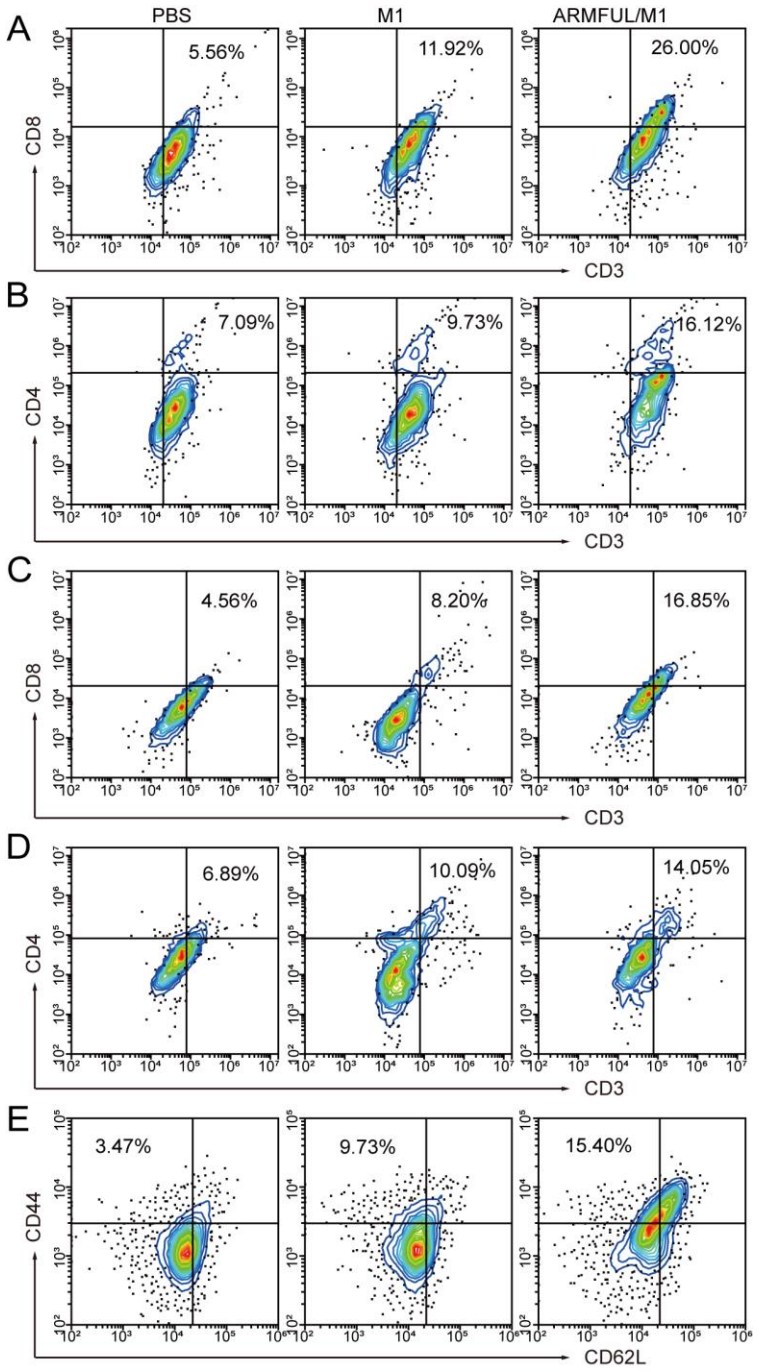

Fig. S22. FACS analysis of T cell activation in tumors and spleens.

(**A**, **B**), The percentage of $CD8^+$ and $CD4^+$ T cells in primary tumors. The cells were gated from $CD45^+$ populations in the FACS profile. (**C**, **D**), The percentage of $CD8^+$ and $CD4^+$ T cells in distant tumors. The cells were gated from $CD45^+$ populations in the FACS profile. (**E**), The percentage of effector memory T cells in the spleen. The $CD62^-CD44^+$ T cells were gated from $CD45^+CD4^+$ populations in the FACS profile.

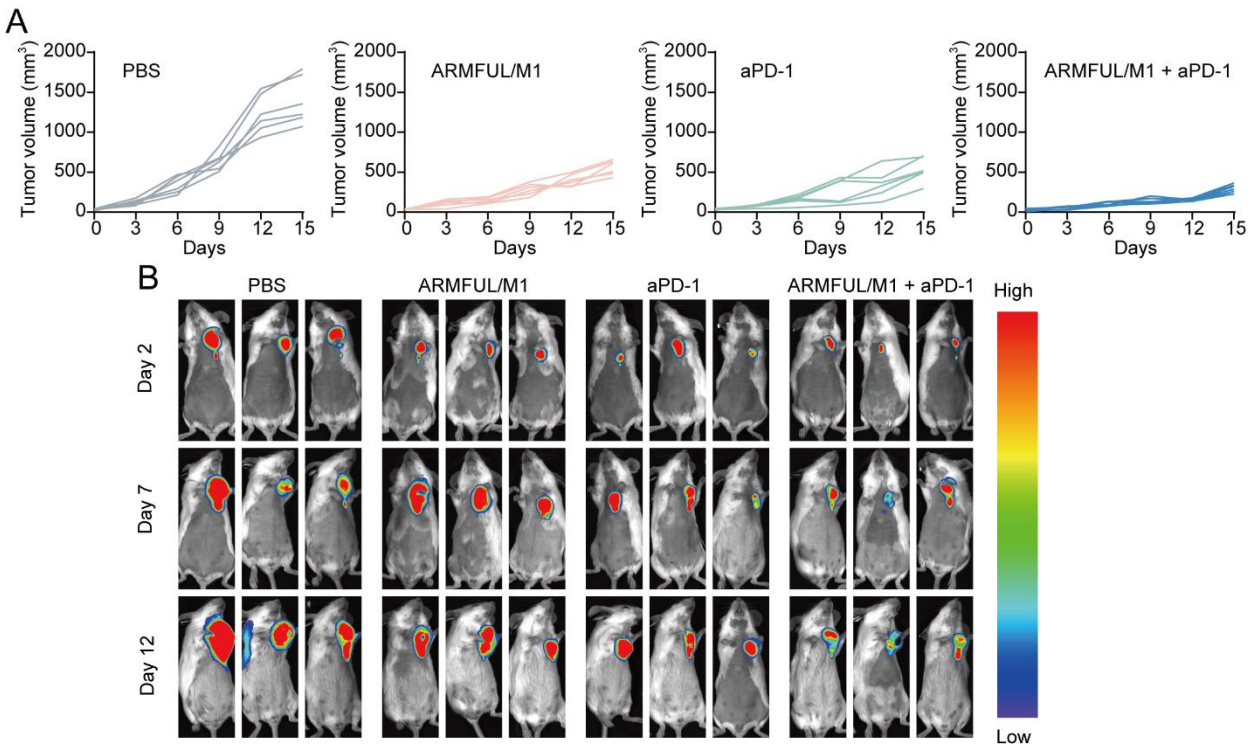

Fig. S23. Individual tumor growth and bioluminescence imaging of mice.

(**A**), Growth curves of tumors in individual mice burdened with 4T1-Luc cells after intravenous injection of PBS, ARMFUL/M1, aPD-1, and ARMFUL/M1 + aPD-1 (n = 6/group). (**B**), *In vivo* bioluminescence imaging of tumor growth of mice burdened with 4T1-Luc cells.

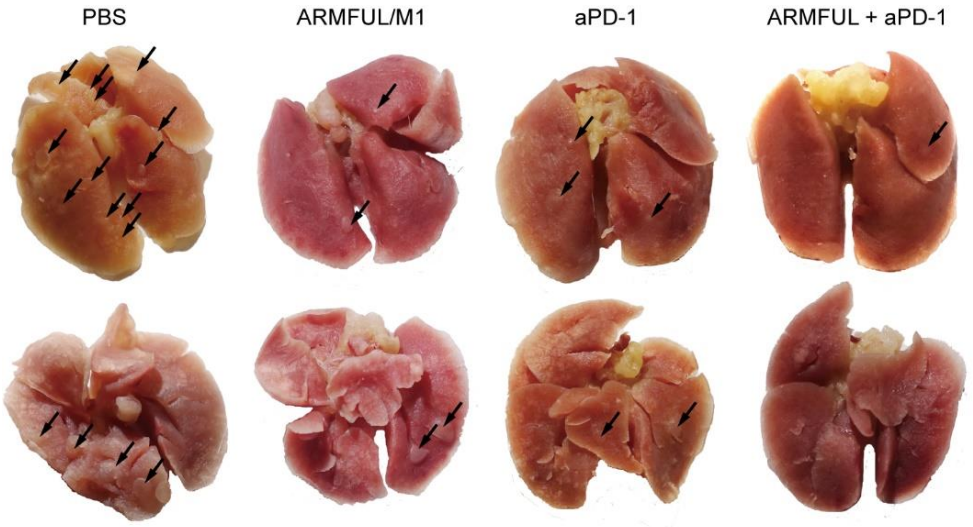

Fig. S24. Representative images of metastatic nodules in the lung after treatment.

Movie S1. Macrophage phagocytosis: natural M1 macrophages cocultured with B16F10 tumor cells.

The views in the plate were recorded through a live cell dynamic imaging and analysis system (zenCELL owl) every 10 minutes for 36 h. In the recorded images, B16F10 tumor cells were fusiform, and macrophages were round, making them distinguishable.

Movie S2. Macrophage phagocytosis: ARMFUL engineered M1 macrophages cocultured with B16F10 tumor cells.

The views in the plate were recorded through a live cell dynamic imaging and analysis system (zenCELL owl) every 10 minutes for 36 h. In the recorded images, B16F10 tumor cells were fusiform, and macrophages were round, making them distinguishable.